



OPEN A nitrogen deprivation gradient triggers transcriptional reprogramming for lipid biosynthesis in *Auxenochlorella pyrenoidosa*

Wang Liufu^{1,2,5}, Ma Xueyan^{1,2,5}, Huang Xuxiong⁴✉, Wen Haibo^{1,2,3}✉, Jin Wu^{1,2,3}, Chen Wanwen^{1,2}, Wang Yufeng^{1,2} & Xu Pao^{1,2,3}

Nitrogen deprivation is a well-established strategy to enhance lipid accumulation in microalgae, yet the transcriptomic mechanisms underlying a gradient of nitrogen deprivation remain poorly understood. This study investigated the oleaginous microalga *Auxenochlorella pyrenoidosa* under a sodium nitrate (NaNO₃) gradient (1.5, 1, 0.5, and 0 g L⁻¹). RNA-seq analysis revealed distinct molecular responses tailored to nitrogen availability. Under mild limitation (1 g L⁻¹), nitrate assimilation and nitrogen metabolism were predominantly suppressed. Moderate deprivation (0.5 g L⁻¹) triggered extensive downregulation of the photosynthetic apparatus, encompassing chloroplast function and porphyrin/chlorophyll metabolism. In contrast, severe deprivation (0 g L⁻¹) induced nucleolar stress and upregulated ribosome biogenesis, indicating a fundamental shift in gene expression regulation. Common adaptive mechanisms across all stress levels included the consistent upregulation of the TCA cycle, MAPK signaling, and specific transporters. Furthermore, series cluster analysis identified monotonically expressed genes implicating tRNA processing, the COP9 signalosome, glycolysis, gibberellin response, and lysosomal hydrolases as potential rate-limiting steps governing lipid accumulation. Our findings provide a comprehensive transcriptomic landscape, revealing both tiered and shared regulatory networks, and propose novel targets for engineering lipid production in microalgae under precision nitrogen regulation.

Keywords Lipid production, Nitrogen concentrations, Transcriptome, Underlying mechanisms

Microalgal lipids mostly consist of saturated and monounsaturated fatty acids, which are promising replaceable sources for biodiesel manufacture¹. Meanwhile, a certain species of microalgae produces polyunsaturated fatty acids (PUFAs) including eicosapentaenoic acid (EPA) and docosahexaenoic acid (DHA). Recently, their positive impacts on the health of humans and animals have made these PUFAs a subject of intense interest². Therefore, the versatility of microalgal lipids as resources for energy, health, and industrial products gives them significant economic and practical value. Nowadays, the main challenge in the mass production of microalgal lipids remains the improvement of lipid accumulation^{3,4}. A valuable approach to solving the problem is metabolic engineering, which is based on the comprehensive understanding of the regulatory mechanisms in the lipid biosynthesis of microalgae⁵. Thus, it is significant to use transcriptome analysis to elucidate the molecular mechanisms underlying lipid accumulation in microalgae. This is beneficial for the development of metabolic engineering, thereby facilitating the technological progress of microalgal lipid production⁶.

¹Key Laboratory of Integrated Rice-Fish Farming Ecology, Ministry of Agriculture and Rural Affairs, Freshwater Fisheries Research Center, Chinese Academy of Fishery Sciences, Wuxi 214081, China. ²Sino-US Cooperative Laboratory for Germplasm Conservation and Utilization of Freshwater Mollusks, Freshwater Fisheries Research Center, Chinese Academy of Fishery Sciences, Wuxi 214081, China. ³Wuxi Fisheries College, Nanjing Agricultural University, Wuxi 214081, China. ⁴Centre for Research on Environmental Ecology and Fish Nutrition (CREEFN) of the Ministry of Agriculture and Rural Affairs, Shanghai Ocean University, Shanghai 201306, China. ⁵Wang Liufu and Ma Xueyan contributed equally to this work. ✉email: Huangxuxiong@163.com; 1103173569@qq.com

Deprivation of environmental nitrogen can effectively affect lipid contents in microalgae⁷. Many studies have shown that partial or complete nitrogen deprivation in the medium induces an increase in lipid content in microalgae. This suggests that different levels of nitrogen deprivation may trigger similar mechanisms to enhance lipid biosynthesis⁸. Moreover, some studies reported that the extent of lipid accumulation varies depending on the degree of nitrogen limitation, suggesting that distinct nitrogen deprivation levels may involve different regulatory mechanisms for lipid biosynthesis^{9–11}. If these similarities and differences can be identified, it will deepen our understanding of the relevant mechanisms to facilitate the use of metabolic engineering to enhance lipid accumulation in microalgae. However, previous studies focused mainly on the molecular mechanism of lipid accumulation in microalgae under nitrogen starvation conditions (i.e. without nitrogen). These studies reported that transcriptional inductions of nitrogen assimilation, tricarboxylic acid (TCA) cycle, pyruvate kinase and a subset of diacylglycerol acyltransferases were important in increasing lipid biosynthesis. At the same time, the transcriptional processes of cellular photosynthesis, gluconeogenesis and translation (ribosomes) were inhibited¹². However, transcriptomic information regarding lipid biosynthesis under moderate or limited nitrogen conditions remains scarce. Therefore, it remains unclear what commonalities and differences exist in the regulatory mechanisms across different levels of nitrogen deprivation¹³.

Auxenochlorella pyrenoidosa, known for its high tolerance to abiotic stresses, is a common and promising species for lipid production¹⁴. Therefore, it was chosen as the subject of this study and exposed to sodium nitrate (NaNO_3) concentrations of 1.5, 1, 0.5 and 0 g L⁻¹ for 5 days. The lipid contents were analyzed and RNA-seq was applied to mRNA libraries to investigate the roles of key biological processes in the lipid accumulation of *A. pyrenoidosa* under varying nitrogen deprivation. This study aims to deepen our understanding of how varying levels of nitrogen deprivation regulate lipid biosynthesis in microalgae.

Methods

Microalgal strain and culture

A. pyrenoidosa SHOU-1002, obtained from a microalgal seed bank at Shanghai Ocean University, was cultured in BG-11 medium (containing 1.5 g L⁻¹ NaNO_3 , analytical grade) for two weeks. The algal culture was harvested during the exponential growth phase and centrifuged (4 °C, 6000 rpm, 3 min) to remove the supernatant. The obtained algal pellet was washed twice with sterile water and then inoculated into 2.5 L BG-11 media with 1.5, 1, 0.5 and 0 g L⁻¹ NaNO_3 in 3 L Erlenmeyer flasks. These flasks were labeled as N1.5 (Ncon), N1, N0.5 and N0 groups, respectively (Table 1). Three replicates were performed for each group, with initial biomass concentrations of approximately 0.8 g L⁻¹. All cultures were incubated in an incubator with photoperiod 12:12 (L: D), temperature 25 °C, light intensity 70 $\mu\text{mol photons}\cdot\text{m}^{-2}\cdot\text{s}^{-1}$. They were shaken 3 times a day manually.

Measurement of exogenous sodium nitrate in media

The nitrate nitrogen was measured using a spectrophotometric method¹⁵. The absorbance of a series of standard solutions at 220 nm and 275 nm (denoted as $A_{(220)}$ and $A_{(275)}$, respectively) was measured using a fluorescence-spectrophotometer (Shimadzu RF-540, Japan) to perform the linear regression and construct the standard curve. The absorbance of the sample was then measured, and the nitrate nitrogen concentration was calculated according to the regression equation. Finally, the concentration of NaNO_3 (g/L) was calculated using the regression equation obtained from the standard curve.

Biochemical analysis

The samples were collected every other day to analyze lipid contents. Cell biomass was harvested by centrifugation at 8000 × g for 10 min from 250 mL culture and washed with sterile water. Then, the algal cells were frozen at -20 °C overnight, followed by vacuum drying (-46 °C, 24 h), then weighed to determine the biomass (B, g L⁻¹). Then, the contents of total lipids were detected as described by Huang et al.⁹. In brief, 0.2 g dried microalgae were extracted using 50 mL chloroform-methanol for 24 h. The extraction process involved pulsed sonication (5 s on, 5 s off) at 60% amplitude (of a 500 W maximum output) and a frequency of 70 Hz intensity and room temperature. After two extraction cycles of 30 min each, the suspension was filtered and the obtained filtrate was washed twice with 0.88% KCl solutions. Subsequently, the lower organic phase was transferred into pre-weighed glass vials, which were dried at 40 °C under vacuum until they reached constant weights. The total lipid contents were assayed in gravimetric (in % dry weight).

Total RNA Preparation and quality test

Three independent biological replicates were used for each treatment group. After 5-days of exposure, the NaNO_3 in the N0.5 group was nearly depleted (Fig. 1). Then, 0.6 g fresh algal cells of each group were harvested to extract total RNA by TRIzol reagent (Invitrogen, USA) according to the manufacturer's protocol. The genomic DNA was removed using RNase-free DNase I (Fermentas, Canada). Total RNA was quantified and assessed

Number	Classification	Definition	Nitrogen concentration	Label
1	control	nitrogen repletion	BG-11 medium (1.5 g L ⁻¹ NaNO_3)	N1.5 (Ncon)
2	treatment	nitrogen limitation	1 g L ⁻¹ NaNO_3	N1
3	treatment	nitrogen limitation	0.5 g L ⁻¹ NaNO_3	N0.5
4	treatment	nitrogen starvation	0 g L ⁻¹ NaNO_3	N0

Table 1. The information of each group in this study.

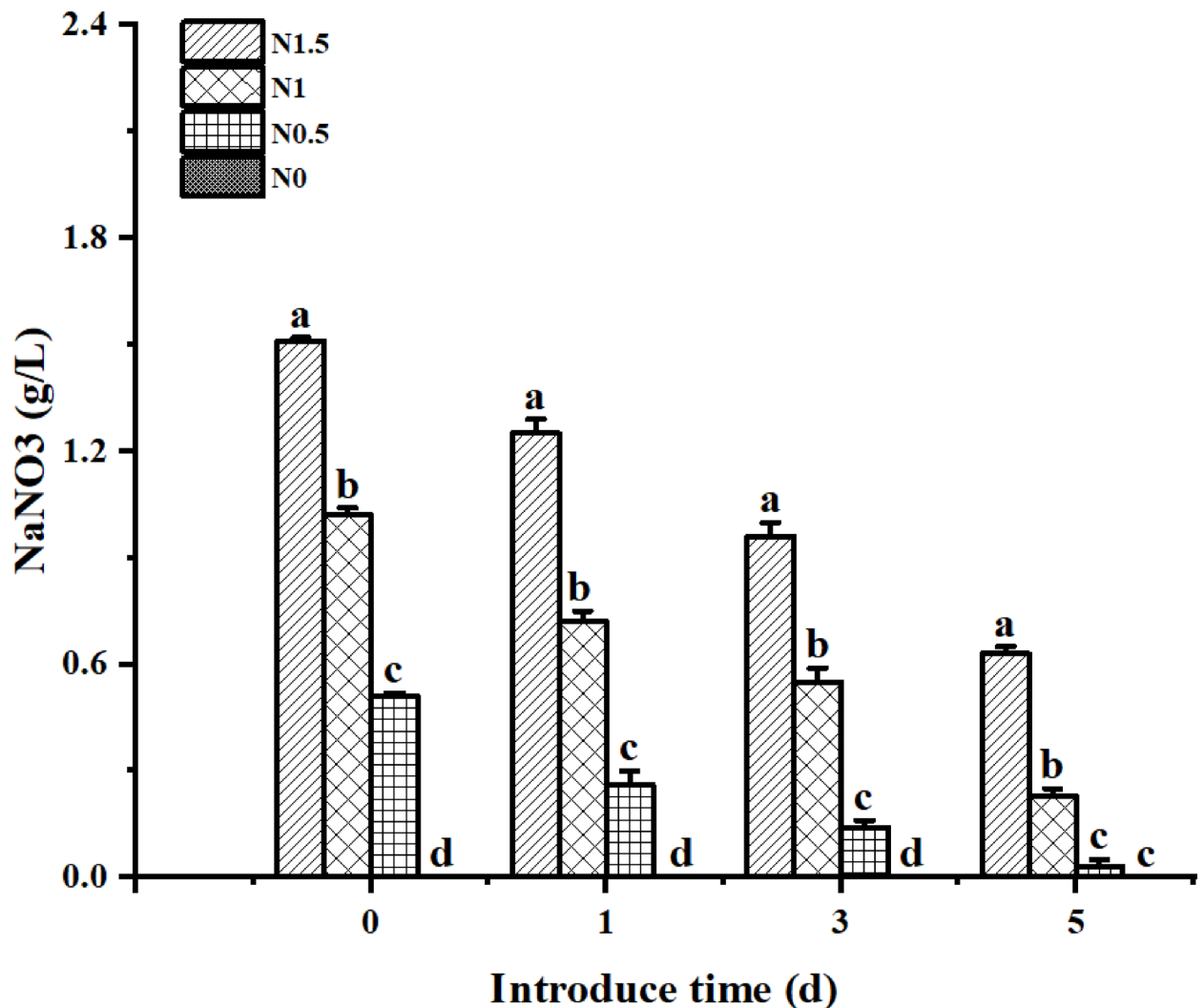


Fig. 1. The concentration of sodium nitrate in media. N1.5, 1.5 g/L NaNO₃ group; N1, 1 g/L NaNO₃ group; N0.5, 0.5 g/L NaNO₃ group; N0, 0 g/L NaNO₃ group. A one-way ANOVA was performed to compare the effects of different treatments within each day. The values with the same or no little letter superscripts mean no significant difference ($P > 0.05$), while those with different little letter superscripts mean significant difference ($P < 0.05$).

for quality as follows. 1% agarose gels were used to monitor the degradation and contamination of total RNA. The NanoPhotometer[®] (IMPLEN, USA) was used to measure the concentration of total RNA. The integrity was assessed through RNA Nano 6000 Assay Kit on the Agilent 2100 Bioanalyzer (Agilent Technologies, USA). The criteria used to select total RNA for subsequent analyses were $OD_{260/280} \geq 1.9$, 28 S/18S rRNA ratio ≥ 1.6 , RIN value ≥ 7.0 , and a minimum required amount and concentration of total RNA were 3 μ g and 50 ng/ μ L, respectively.

mRNA-seq library construction and sequencing

Twelve libraries from Ncon (Ncon-1, Ncon-2 and Ncon-3), N1 (N1-1, N1-2 and N1-3), N0.5 (N0.5-1, N0.5-2 and N0.5-3) and N0 (N0-1, N0-2 and N0-3) were constructed. Briefly, oligo (dT) magnetic beads (Yeasen, China) were added to purify mRNA from total RNA. The fragmenting of mRNA and the synthesis of double stranded cDNA were completed using the NEBNext[®] Ultra[™] RNA Library Prep Kit for Illumina[®] (NEB, USA). The samples obtained were purified using PCR purification kits (Takara, Japan). After adenylation and end-filling by Hieff NGS[®] Ultima[™] Endprep Mix (Yeasen, China), the adapters were ligated to the cDNA by Hieff NGS[®] Ultima[™] DNA Ligation Module (Yeasen, China) and fragment sizes were verified by agarose gel electrophoresis. 150 bp fragments were selected using the AMPure XP system (Beckman Coulter, Beverly, USA) for PCR amplification: 1 cycle of 98 °C for 30 s and then 10 cycles of 98 °C for 10 s each, followed by 65 °C for 30 s, and 72 °C for 30 s. Finally, a 5-min extension step was performed at 72 °C. After that, all libraries were sequenced on an Illumina HiSeq[™] 2500 platform. The raw data of the transcriptome have been submitted to the National Center for Biotechnology Information (<https://www.ncbi.nlm.nih.gov/search/all/?term=GSE233967>).

Bioinformatic analysis

The read filtering, unigene counting, Venn analysis, Gene ontology (GO) analysis, Kyoto Encyclopedia of Genes and Genomes (KEGG) analysis, gene co-expression network and series cluster were carried out according to Zhang et al.¹⁶. Raw sequencing data in FASTQ format were first processed using Trimmomatic. Reads containing poly-N regions and low-quality reads were removed to obtain the clean reads. After removing adapters and low-quality sequences, the clean reads were assembled de novo into contigs and transcripts by Trinity (version 2.4) using the paired-end sequencing approach. The longest transcript was chosen as a unigene based on the similarity and length for subsequent analyses.

In particular, differentially expressed genes (DEGs) were identified using Baggerley's test with default filtering conditions. FPKM and read counts value of each unigene were calculated using bowtie2 and eXpress. DEGs were identified using the DESeq2 functions estimateSizeFactors and nbinomTest. The thresholds were set as a false discovery rate (FDR) ≤ 0.05 and an absolute Log₂ fold change (FC) ≥ 1 . Hierarchical cluster analysis of DEGs was performed to explore transcripts expression pattern. GO enrichment and KEGG pathway enrichment analysis of DEGs were respectively performed using R based on the hypergeometric distribution. A p-value ≤ 0.05 was considered statistically significant for hypergeometric tests in GO analysis, KEGG analysis, and series clustering. Gene pairs showing significant correlation (p-value ≤ 0.05) were used to construct the co-expression network^{17,18}.

Quantitative real-time PCR (qRT-PCR) verification

Six genes from each treatment were chosen for qRT-PCR. The same RNA extracts utilized for RNA-seq were also employed to analyze the target genes. The primers were designed using the Primer 5 software (Supplementary data Table S1) and the actin (ACT) gene was selected as the internal reference gene. DEPC water was used to substitute for cDNA in the negative control groups. The qRT-PCR was performed using Agilent AriaMx qRT-PCR System. The reaction systems contained 10 μ L SYBR Green Master Mix (YEASEN Biotech, Shanghai, China), 0.4 μ L of each forward and reverse primer (10 nmol), 1 μ L cDNA, and 8.2 μ L DEPC-treated water. The qRT-PCR protocol included an initial denaturation at 95 °C for 2 min, followed by 30 cycles of 95 °C for 10 s and 60 °C for 20 s. Finally, a melting curve analysis was conducted. $2^{-\Delta\Delta CT}$ method was applied to calculate the average threshold cycle (Ct) of gene expression (Supplementary data Table S2), which was then normalized¹⁶.

Statistical analysis

The lipid contents were presented as mean \pm standard error. Significant differences among groups were assessed using one-way ANOVA in SPSS software (Version 11.0), after confirming normality and homogeneity of variances. Post-hoc multiple comparisons were performed using Duncan's test and a significant level of p-value ≤ 0.05 was selected.

Results

Changes in lipid contents of microalgae under varying nitrogen deprivation

Over time, the effects of varying nitrogen deprivation on lipid contents in microalgae gradually became apparent. After 5 days, *A. pyrenoidosa* cultured in the 1.5 g L⁻¹ NaNO₃ group exhibited the lowest lipid content (11.82%). In contrast, higher lipid contents were observed in cultures supplemented with 1 g L⁻¹, 0.5 g L⁻¹, and 0 g L⁻¹ NaNO₃, with values of 14.18%, 18.95%, and 22.81%, respectively (Fig. 2). These results demonstrate a clear inverse relationship between nitrate concentration and lipid accumulation, with more severe nitrogen deprivation leading to greater lipid production.

Transcriptomic statistics

A total of 46.65–51.70 million raw reads were obtained. After removing low quality reads, approximately 46.61–51.66 million clean reads were generated in total. Quality analysis indicated that valid base percentages and Q30 values exceeded 98.37% and 90.48%, respectively, in all samples (Supplementary data Table S3). There was no significant difference in the data among the different treatment groups. Finally, 16,415 unigenes were assembled, with a total length of 28,388,667 bp and an average length of 1,729 bp. Specifically, Groups N0.5 and N0 produced the highest and statistically similar unigene counts, which were significantly greater than that of Group N1.5 (p < 0.05) (Supplementary data Table S4). The proportion of complete and single-copy BUSCOs reached 85.48%, indicating a high-quality transcriptome assembly.

DEGs in response to varying nitrogen deprivation

In the 1 g L⁻¹ NaNO₃ group, total 352 DEGs were detected in microalgae, consisting of 168 significantly upregulated genes and 184 significantly downregulated genes. There were 1,976 significantly upregulated genes and 1,245 significantly down-regulated genes in the 0.5 g L⁻¹ NaNO₃ group. At 0 g L⁻¹ NaNO₃, 1,716 genes were significantly upregulated and 1,650 genes were downregulated in microalgae. Venn diagram analysis revealed that 133 genes exhibited differential expression across the three nitrogen deprivation groups, including 70 co-upregulated genes and 26 co-downregulated genes (Figure S1). Figure 3A and C illustrates the distribution and levels of DEGs, highlighting changes in gene expression. Dot plots of gene ontology analysis identified nucleolus, chloroplast, and nitrate assimilation as the most represented pathways (Fig. 3D and F). A key finding is that the number of DEGs increased dramatically with the severity of nitrogen limitation, and a core set of 133 genes responded consistently across all deprivation levels, suggesting their fundamental role in the nitrogen stress response.

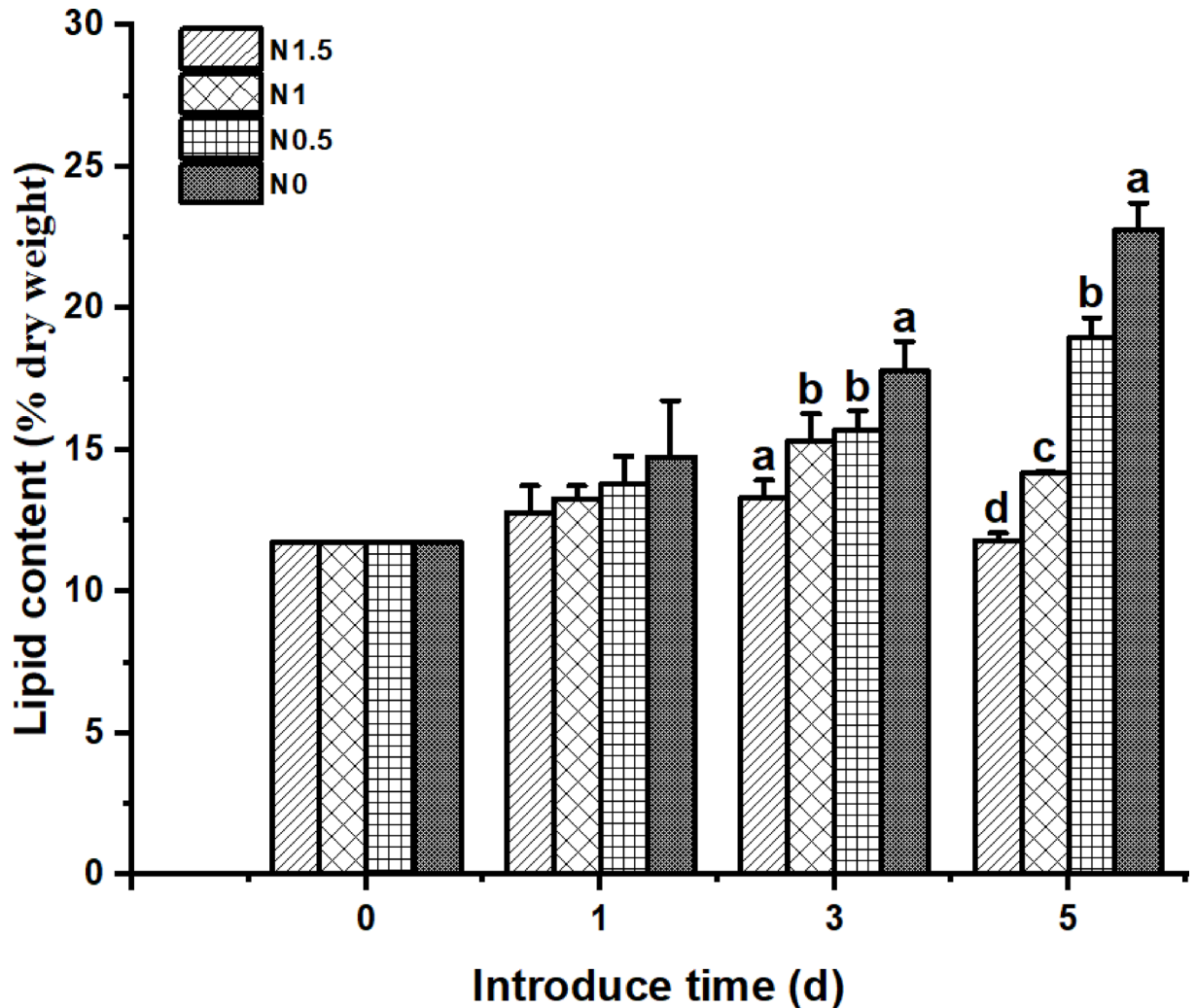


Fig. 2. Effects of different nitrogen concentrations on lipid contents in *A. pyrenoidosa*. N1.5, 1.5 g/L NaNO₃ group; N1, 1 g/L NaNO₃ group; N0.5, 0.5 g/L NaNO₃ group; N0, 0 g/L NaNO₃ group. A one-way ANOVA was performed to compare the effects of different treatments within each day. The values with the same or no little letter superscripts mean no significant difference ($P > 0.05$), while those with different little letter superscripts mean significant difference ($P < 0.05$).

GO and KEGG classification of DEGs under varying nitrogen deprivation

The top ten significantly enriched GO terms in microalgae treated with 1 g L⁻¹, 0.5 g L⁻¹, and 0 g L⁻¹ NaNO₃ are shown in Table 2. Nitrate assimilation (GO:0042128) was the most significantly enriched term in the 1 g L⁻¹ NaNO₃ treated group. For the 0.5 g L⁻¹ NaNO₃ treated group, the most significantly enriched GO term was chloroplast (GO:0009507). In the nitrogen-deprived group (0 g L⁻¹ NaNO₃), the most significantly enriched GO term was nucleolus (GO:0005730).

The top ten significantly enriched KEGG pathways are presented in Table 3. Nitrogen metabolism (ko00910) was the most significantly enriched pathway in the 1 g L⁻¹ NaNO₃ treated group. Under 0.5 g L⁻¹ NaNO₃ treatment, porphyrin and chlorophyll metabolism (ko00860) emerged as the most significantly enriched pathway. Notably, ribosome biogenesis in eukaryotes (ko03008) was ranked second among the top ten significantly enriched KEGG pathways in the 0 g L⁻¹ NaNO₃ treated group.

These analyses revealed that the molecular response to nitrogen deprivation is highly dependent on its severity, shifting from nitrogen salvage and metabolism under mild deprivation to fundamental reorganization of chloroplast function and ribosomal assembly under severe deprivation.

Differential gene expression in key metabolic pathways under varying nitrogen deprivation

Transcriptome analysis of *A. pyrenoidosa* SHOU-1002 under varying nitrogen deprivation revealed significant differential expression of genes involved in central carbon and lipid metabolism. Key findings are summarized in Table 4.

In the Calvin cycle, genes encoding the ribulose biphosphate carboxylase large chain (rbcL), ribulose biphosphate carboxylase small chain (rbcS), phosphoribulokinase (PRK) and sedoheptulose-1,7-biphosphatase

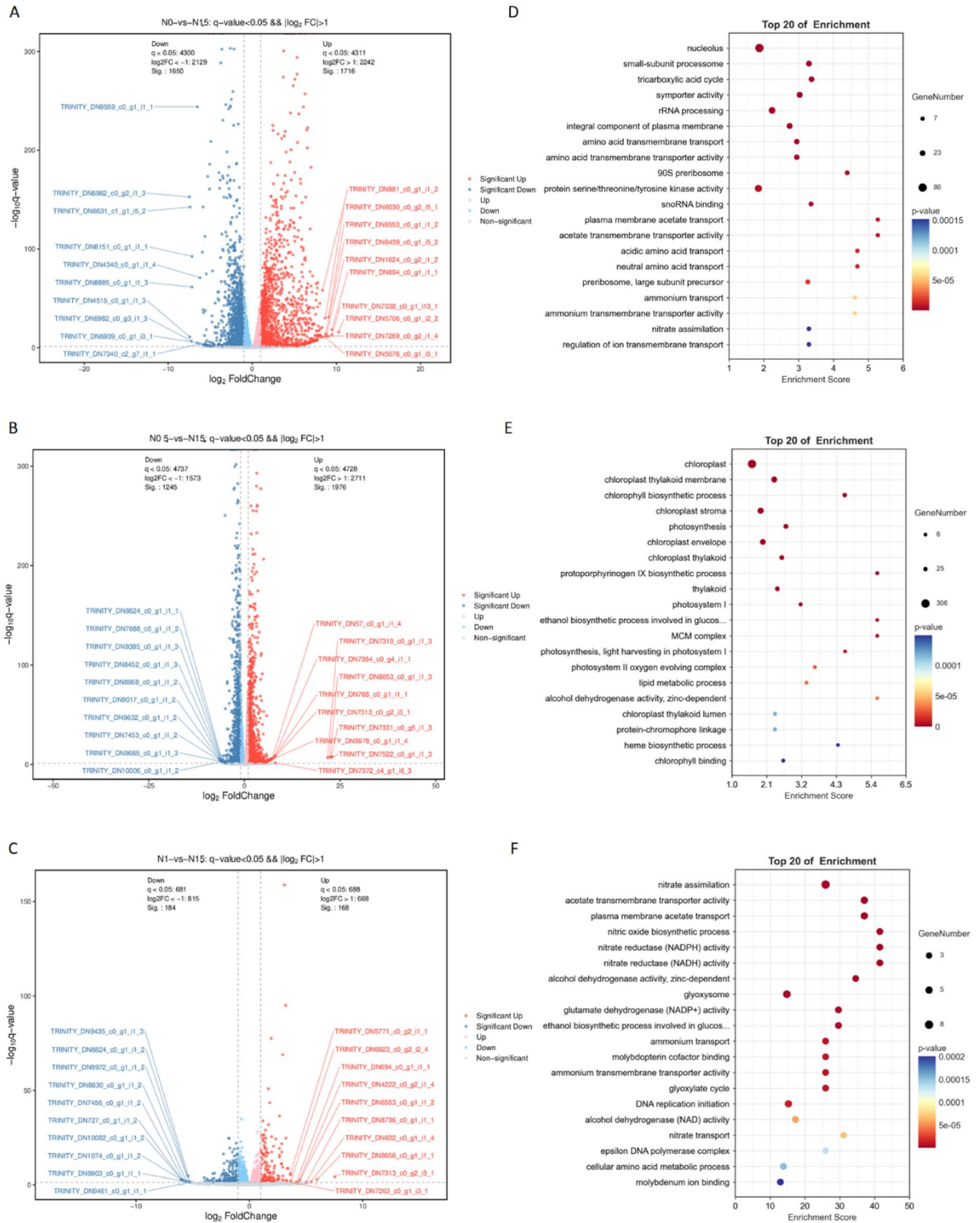


Fig. 3. Transcriptome sequencing analysis of *A. pyrenoidosa* SHOU-1002. The different panels represent: (A-C) a volcano plot displaying the differentially expressed genes and (D-F) a dot plot displaying the gene ontology for differentially expressed genes of *A. pyrenoidosa* SHOU-1002 under varying nitrogen deprivation.

(SBPase) were significantly downregulated. Conversely, genes encoding key glycolytic enzymes, including hexokinase (HK), phosphofructokinase (PFK) and pyruvate kinase (PK), were upregulated.

Within the TCA cycle, the gene expression of the pyruvate dehydrogenase (aceE) and malate dehydrogenase (MDH) was increased, while the gene expression of citrate synthase (CIS) and isocitrate dehydrogenase (IDH) was downregulated. For lipid metabolic pathways, the expression of the glycerol-3-phosphate acyltransferase

Group	GO Id	GO Term	Up-gene	Down-gene	p-value	FDR
N1 vs. N1.5	GO:0042128	nitrate assimilation	0	8	1.72E-10	4.74E-08
	GO:0006847	plasma membrane acetate transport	5	0	5.01E-08	4.59E-06
	GO:0015123	acetate transmembrane transporter activity	5	0	5.01E-08	4.59E-06
	GO:0006809	nitric oxide biosynthetic process	0	4	6.49E-07	2.98E-05
	GO:0009703	nitrate reductase (NADH) activity	0	4	6.49E-07	2.98E-05
	GO:0050464	nitrate reductase (NADPH) activity	0	4	6.49E-07	2.98E-05
	GO:0004024	alcohol dehydrogenase activity, zinc-dependent	4	0	1.92E-06	6.70E-05
	GO:0009514	glyoxysome	6	0	1.95E-06	6.70E-05
	GO:0043458	ethanol biosynthetic process involved in glucose fermentation to ethanol	4	0	4.41E-06	0.000121
	GO:0004354	glutamate dehydrogenase (NADP+) activity	3	1	4.41E-06	0.000121
N0.5 vs N1.5	GO:0009507	chloroplast	72	234	1.99E-23	2.25E-20
	GO:0009535	chloroplast thylakoid membrane	10	89	1.62E-18	9.14E-16
	GO:0015995	chlorophyll biosynthetic process	0	31	1.62E-17	6.10E-15
	GO:0009570	chloroplast stroma	24	84	8.68E-13	2.45E-10
	GO:0015979	photosynthesis	10	35	1.15E-11	2.59E-09
	GO:0009941	chloroplast envelope	18	70	1.40E-11	2.63E-09
	GO:0009534	chloroplast thylakoid	2	39	6.48E-10	1.05E-07
	GO:0006782	protoporphyrinogen IX biosynthetic process	0	12	1.01E-09	1.43E-07
	GO:0009579	thylakoid	3	34	2.96E-08	3.72E-06
	GO:0009522	photosystem I	0	17	1.98E-06	0.000223
N0 vs. N1.5	GO:0005730	nucleolus	5	81	4.20E-10	4.79E-07
	GO:0032040	small-subunit processome	0	25	1.50E-09	8.53E-07
	GO:0006099	tricarboxylic acid cycle	23	0	3.69E-09	1.33E-06
	GO:0015293	symporter activity	22	5	4.68E-09	1.33E-06
	GO:0006364	rRNA processing	1	41	5.19E-08	1.18E-05
	GO:0005887	integral component of plasma membrane	20	6	1.43E-07	2.72E-05
	GO:0003333	amino acid transmembrane transport	18	1	1.68E-06	0.000238
	GO:0015171	amino acid transmembrane transporter activity	18	1	1.68E-06	0.000238
	GO:0030686	90 S preribosome	0	10	2.64E-06	0.000333
	GO:0004712	protein serine/threonine/tyrosine kinase activity	30	19	4.34E-06	0.000494

Table 2. Top ten of significantly clustered GO terms.

(GPAT), lysophosphatidic acid acyltransferase (LPAAT), diacylglycerol acyltransferase (DGAT), phosphatidic acid phosphatase (PAP), acetyl-CoA carboxylase (ACC), malonyl-CoA: ACP transacylase (fabD), and β -Ketoacyl-ACP synthase (fabF) was significantly upregulated.

Collectively, these expression shifts indicate a major metabolic rewiring where carbon flux is redirected from photosynthesis and partial TCA cycle activity towards glycolysis and the robust upregulation of the entire lipid biosynthesis machinery.

qRT-PCR verification

Although the fold-change values differed between qRT-PCR and RNA-seq, the expression trends of the selected genes were consistent across both methods (Supplementary data Figure S2). Generally, the results of these platforms were in agreement, indicating the reliability and validity of the RNA-seq results.

Co-expression network of DEGs under varying nitrogen deprivation

The co-expression network of DEGs included total 45 genes in this study (Fig. 4). SFC1 (mitochondrial succinate-fumarate transporter 1 T10O8.50), C1SY3 (citrate synthase 3, peroxisomal F7D19.21), CYSZ (citrate synthase, glyoxysomal) and MASY (Malate synthase, glyoxysomal NCU10007) had the highest degree of 37, followed by EDR1 (serine/threonine-protein kinase EDR1 F22O13.20) and YHA8 (Uncharacterized transporter YHL008C) with a degree of 27. Network analysis shows that these genes play pivotal roles in coordinating the global transcriptional response to nitrogen deprivation.

Series cluster of DEGs under varying nitrogen deprivation

Total 50 unique model expression tendencies were found (Supplementary data Figure S3). Profile 9 and profile 42 had P-values less than 0.01, and their trends changed monotonically (Fig. 5). The gene cluster in profile 9 was downregulated while the gene cluster in profile 42 was upregulated. These changes were induced by 1 g L^{-1} , 0.5 g L^{-1} and $0 \text{ g L}^{-1} \text{ NaNO}_3$. Moreover, the genes in profile 9 played a significant role in various biological processes, including tRNA processing (GO:0008033), hydrolase activity (GO:0016787), NAD^+ diphosphatase activity (GO:0000210), protein deneddylation (GO:0000338) and COP9 signalosome (GO:0008180). Genes in profile

Group	Pathway Id	Pathway Term	Up-gene	Down-gene	p-value	FDR
N1 vs. N1.5	ko00910	Nitrogen metabolism	1	8	3.56E-11	1.49E-09
	ko03030	DNA replication	0	9	2.93E-08	6.16E-07
	ko03410	Base excision repair	1	4	0.000376	0.005272
	ko00280	Valine, leucine and isoleucine degradation	5	0	0.000541	0.005683
	ko00900	Terpenoid backbone biosynthesis	3	1	0.002613	0.021951
	ko00903	Limonene and pinene degradation	2	0	0.004071	0.028503
	ko03420	Nucleotide excision repair	0	4	0.010946	0.061409
	ko00650	Butanoate metabolism	2	0	0.011697	0.061409
	ko00220	Arginine biosynthesis	1	2	0.014864	0.065575
	ko00010	Glycolysis / Gluconeogenesis	5	0	0.015613	0.065575
N0.5 vs. N1.5	ko00860	Porphyrin and chlorophyll metabolism	3	27	3.79E-10	4.05E-08
	ko00196	Photosynthesis - antenna proteins	0	14	1.43E-06	7.68E-05
	ko00195	Photosynthesis	3	26	2.42E-06	8.64E-05
	ko00710	Carbon fixation in photosynthetic organisms	10	13	0.000200	0.005364
	ko00910	Nitrogen metabolism	4	8	0.000251	0.005391
	ko03030	DNA replication	9	9	0.000542	0.009682
	ko00900	Terpenoid backbone biosynthesis	5	10	0.000666	0.010185
	ko00620	Pyruvate metabolism	17	7	0.001002	0.013408
	ko00010	Glycolysis / Gluconeogenesis	14	12	0.006685	0.079479
	ko00130	Ubiquinone and other terpenoid-quinone biosynthesis	2	7	0.011609	0.111337
N0 vs. N1.5	ko00220	Arginine biosynthesis	17	4	5.28E-10	5.39E-08
	ko03008	Ribosome biogenesis in eukaryotes	2	32	2.46E-09	1.05E-07
	ko00910	Nitrogen metabolism	13	4	3.09E-09	1.05E-07
	ko00020	Citrate cycle (TCA cycle)	21	2	4.71E-07	1.20E-05
	ko00053	Ascorbate and aldarate metabolism	8	6	1.23E-05	0.000251
	ko00620	Pyruvate metabolism	19	6	0.000137	0.002330
	ko00250	Alanine, aspartate and glutamate metabolism	9	6	0.000220	0.003210
	ko00230	Purine metabolism	16	13	0.000261	0.003334
	ko00410	beta-Alanine metabolism	11	2	0.000719	0.007782
	ko00903	Limonene and pinene degradation	5	0	0.000780	0.007782

Table 3. Top ten of significantly clustered KEGG pathways.

Transcript_id	Metabolic pathway	Protein	Expression changes	p-value	FDR
TRINITY_DN1021_c0_g1_i2_3	Calvin cycle	Ribulose biphosphate carboxylase large chain (rbcL)	Down	8.23E-15	5.37E-14
TRINITY_DN1392_c0_g1_i1_1		Ribulose biphosphate carboxylase small chain (rbcS)	Down	1.20E-14	7.73E-14
TRINITY_DN2400_c0_g1_i1_2		Phosphoribulokinase (PRK)	Down	9.18E-17	6.71E-16
TRINITY_DN3879_c0_g1_i2_4		Sedoheptulose-1,7-bisphosphatase (SBPase)	Down	2.50E-09	1.11E-08
TRINITY_DN5924_c0_g1_i3_3	Glycolysis	Hexokinase (HK)	Up	9.38E-09	3.99E-08
TRINITY_DN4190_c0_g1_i1_1		Phosphofructokinase (PFK)	Up	1.07E-07	4.18E-07
TRINITY_DN774_c0_g1_i1_1		Pyruvate kinase (PK)	Up	3.50E-07	1.30E-06
TRINITY_DN1331_c0_g1_i1_1	TCA cycle	Pyruvate dehydrogenase (aceE)	Up	2.91E-06	9.93E-06
TRINITY_DN6504_c0_g1_i2_1		Citrate synthase (CIS)	Down	4.40E-06	1.47E-05
TRINITY_DN5433_c0_g1_i2_4		Isocitrate dehydrogenase (IDH)	Down	5.12E-05	1.52E-04
TRINITY_DN5943_c0_g1_i1_3		Malate dehydrogenase (MDH)	Up	2.11E-04	5.75E-04
TRINITY_DN5081_c0_g1_i2_4	Kennedy	Glycerol-3-phosphate acyltransferase (GPAT)	Up	3.71E-04	9.78E-04
TRINITY_DN513_c0_g1_i1_2		Lysophosphatidic acid acyltransferase (LPAAT)	Up	6.21E-04	1.59E-03
TRINITY_DN7223_c0_g2_i1_3		Diacylglycerol acyltransferase (DGAT)	Up	6.79E-04	1.73E-03
TRINITY_DN5241_c0_g2_i3_4		Phosphatidic acid phosphatase (PAP)	Up	8.53E-04	2.14E-03
TRINITY_DN6859_c0_g1_i9_2		Acetyl-CoA carboxylase (ACC)	Up	3.78E-03	8.50E-03
TRINITY_DN7324_c0_g1_i4_1		Malonyl-CoA: ACP transacylase (fabD)	Up	4.99E-03	1.10E-02
TRINITY_DN3386_c1_g1_i1_1		β-Ketoacyl-ACP synthase (fabF)	Up	1.05E-02	2.15E-02

Table 4. Differentially expressed genes of key metabolic pathways in *A. pyrenoidosa* SHOU-1002 under varying nitrogen deprivation (N1, N0.5 and N0 groups).

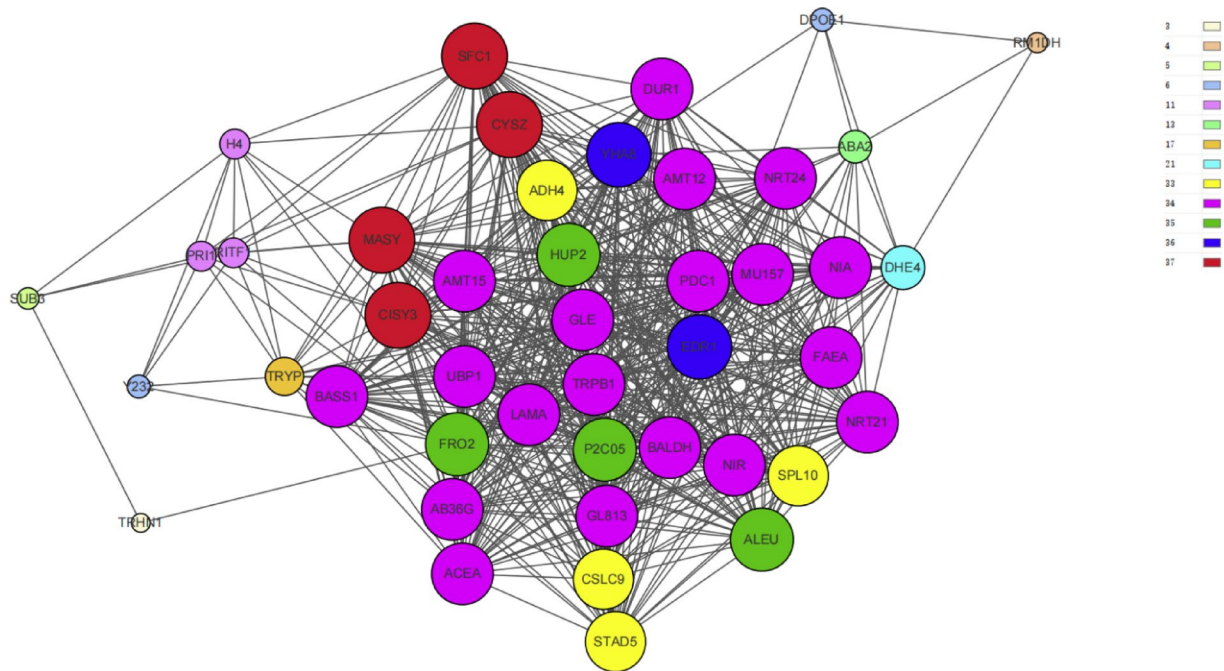


Fig. 4. Co-expression network of DEGs from N1, N0.5 and N0 groups. Different color from 3–37 represents varying degree centrality, where the higher degree centrality stands for the more importance of a gene.

AMT15: Putative ammonium transporter 1 member 5 K7M2.6; AB36G: ABC transporter G family member 36 P0410E03.7; ADH4: Alcohol dehydrogenase 4 SPAC5H10.06c; ACEA: Isocitrate lyase CC1G_07122; ACEA: Isocitrate lyase ICL; ABA2: Zeaxanthin epoxidase, chloroplastic ABA2; AMT12: Ammonium transporter 1 member 2 F13O11.9; ALEU: Thiol protease aleurain; BASS1: Probable sodium/metabolite cotransporter BASS1, chloroplastic T30F21.11; BALDH: Benzaldehyde dehydrogenase, mitochondrial BALDH; CSLC9: Probable xyloglucan glycosyltransferase 9 OSJNBa0072F13.8; CYS3: Citrate synthase 3, peroxisomal F7D19.21; CYSZ: Citrate synthase, glyoxysomal; DPOE1: DNA polymerase epsilon catalytic subunit A T23G18.21; DUR1: Allophanate hydrolase YBR1448; DHE4: NADP-specific glutamate dehydrogenase; EDR1: Serine/threonine-protein kinase EDR1 F22O13.20; FRO2: Ferric reduction oxidase 2 F22L4.12; FAEA: Probable feruloyl esterase A AFLA_066140; GLE: Autolysin; GL813: Germin-like protein 8–13 OsJ_026468; HUP2: H(+)/hexose cotransporter 2 HUP2; H4: Histone H4 MMN10.22; LAMA: Putative urea carboxylase AN0887; MU157: Meiotically up-regulated gene 157 protein SPAC12B10.16c; MASZ: Malate synthase, glyoxysomal NCU10007; NRT21: High-affinity nitrate transporter 2.1 OJ1399_H05.5; NIR: Ferredoxin–nitrite reductase, chloroplastic NIR; NRT24: High affinity nitrate transporter 2.4 MAE1.2; NIA: Nitrate reductase [NADH] NITA; P2C05: Probable protein phosphatase 2 C 5 T12M4.15; PDC1: Pyruvate decarboxylase 1 OsI_019612; PRI1: DNA primase small subunit SPAC6B12.10c; RITF1: Protein RGF1 INDUCIBLE TRANSCRIPTION FACTOR 1 T4E5; RM1DH: L-rhamnose-1-dehydrogenase PICST_50944; STAD5: Stearoyl-[acyl-carrier-protein] 9-desaturase 5, chloroplastic OsJ_14516; SFC1: Mitochondrial succinate-fumarate transporter 1 T10O8.50; SPL10: Squamosa promoter-binding-like protein 10 B1047G05.25; SUB3: Subtilisin-like protease 3 SUB3; TRHN1: Group 1 truncated hemoglobin LI637 LI637; TRPB1: Tryptophan synthase beta chain 1, chloroplastic MBG8.7; TRYP: Trypsin; UBP1: Oligouridylylate-binding protein 1 UBP1; Y232: Glycosyltransferase family 92 protein RCOM_0530710 RCOM_0699480; YHA8: Uncharacterized transporter YHL008C YHL008C.

42 mostly enriched in response to gibberellin (GO:0009739), thiamine pyrophosphate binding (GO:0030976), TCA cycle (GO:0006099), succinate dehydrogenase activity (GO:0000104), pyruvate decarboxylase activity (GO:0004737), mitochondrial electron transport, succinate to ubiquinone (GO:0006121), hydrolase activity, acting on carbon-nitrogen (but not peptide) bonds (GO:0016810) related GO terms. Two gene clusters with statistically significant and monotonically changing expression patterns were identified, representing a suite of co-regulated genes that are systematically suppressed or activated in direct proportion to the degree of nitrogen deprivation.

Discussion

We conducted 5-days exposure of *A. pyrenoidosa* under a series of 1.5, 1, 0.5 and 0 g·L⁻¹ NaNO₃. With the decrease in nitrogen concentrations, the final lipid contents showed a stepwise increase (Fig. 2). The significantly higher number of unigenes in the N0.5 and N0 groups indicates a greater transcriptome complexity, which likely reflects a more active and diverse gene expression profile under these specific conditions. Moreover, the Venn diagram revealed both unique and shared DEGs among microalgae under different nitrogen concentrations (Supplementary data Figure S1). Based on the results of GO analysis and KEGG analysis, we aimed to uncover

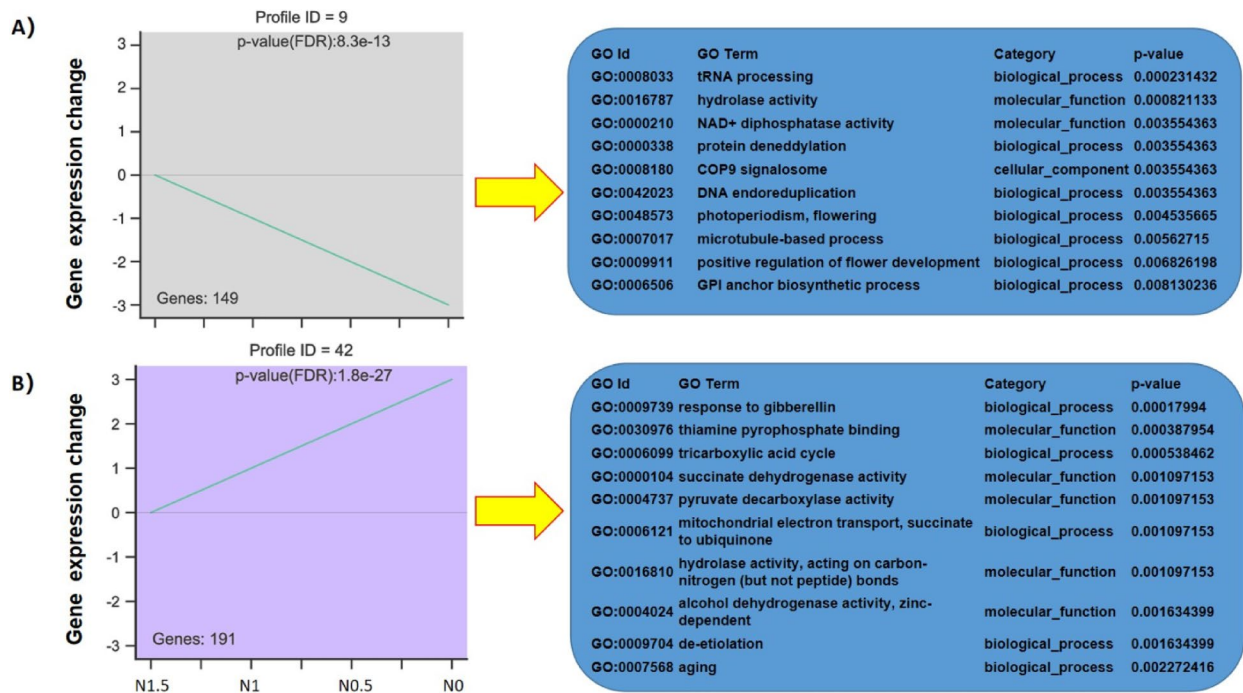


Fig. 5. Gene clusters and top ten GO terms of profile 9 (A) and profile 42 (B). The horizontal axis shows N1.5, N1, N0.5 and N0 groups, and the vertical axis represents the expression levels for genes after Log normalized transformation.

distinct regulatory mechanisms in the lipid accumulation of *A. pyrenoidosa* under varying nitrogen deprivation. Furthermore, the co-expression network was used to reveal common regulatory mechanisms. Furthermore, potential rate-limiting steps in these regulatory mechanisms were identified based on the series cluster analysis.

Distinct characteristics of regulatory mechanisms at different nitrogen concentrations

In this study, our GO enrichment analysis revealed that the most significantly altered biological processes under varying nitrogen concentrations were nitrogen assimilation (Profile N1), chloroplast metabolism (Profile N0.5), and nucleolar stress (Profile N0) (Table 2). These processes collectively regulate lipid biosynthesis by modulating the availability of carbon skeletons and energy. Specifically, the carbon skeleton alpha-ketoglutarate and adenosine triphosphate (ATP) are essential for nitrogen assimilation. Inhibition of nitrogen assimilation leads to accumulation of carbon skeletons and ATP, which can be redirected toward lipid biosynthesis¹⁹. Similarly, chloroplast metabolism affects lipid accumulation by altering the production of ATP and reducing nicotinamide adenine dinucleotide phosphate (NADPH)²⁰. Moreover, nucleolar stress activates a distinct lipogenesis pathway to redirect excessive energy toward lipid storage²¹.

Complementarily, KEGG pathway analysis further confirmed these findings at the metabolic network level, identifying significantly enriched pathways including nitrogen metabolism (across all groups), photosynthesis and porphyrin/chlorophyll metabolism (N0.5), and the TCA cycle and ribosome biogenesis (N0) (Table 3). The consistent alteration in nitrogen metabolism pathways across gradients underscores its central role, while the distinct pathway enrichments specific to each nitrogen level—such as the downregulation of photosynthetic components in N0.5 and the activation of the TCA cycle in N0—reflect a graded metabolic reprogramming. This coordinated shift at the pathway level supports the notion that carbon and energy fluxes are fine-tuned to optimize lipid accumulation under different stress intensities²².

Common characteristics of regulatory mechanisms at different nitrogen concentrations

As shown in Fig. 4, the genes of the TCA cycle (i.e. SFC1, CYSY3, CYSZ and MASY) had the highest degree centrality, followed by genes encoding MAPK and transporters (i.e. EDR1 and YHA8). These results suggest that the TCA cycle, MAPK cascade, and transporters play conserved roles in lipid accumulation of microalgae under varying nitrogen deprivation. Under the condition of nitrogen starvation, membrane and intracellular transporters play roles in cellular homeostasis. For example, the redistribution of intracellular carbon fluxes occurs, ultimately yielding acetyl-CoA or succinyl-CoA as intermediates in the TCA cycle. These intermediates enter the TCA cycle, which channels carbon flux toward lipid biosynthesis²³. Mitogen-activated protein kinase (MAPK) cascade activates lipogenic genes through transcription factors to enhance lipid biosynthesis in microalgae²⁴. These regulatory processes should also apply to lipid biosynthesis in microalgae under other nitrogen deprivation, which is supported by the co-expression network in this study. The centrality of these genes in the network suggests that the TCA cycle, MAPK cascade, and transporters play conserved roles in lipid accumulation of microalgae under varying nitrogen deprivation. The activity of these pathways may be

modulated by reactive oxygen species (ROS) generated under nitrogen deprivation. It is known that varying nitrogen deprivation can affect electron transport chains in mitochondria and chloroplasts to increase ROS. When ROS levels reach a certain threshold, essential molecules can accumulate through the TCA cycle and transporters. Additionally, gene expression can be upregulated through MAPK cascades to enhance lipid accumulation²⁵.

Critically, our findings showed that the consistent activation of the MAPK cascade across nitrogen regimes establishes it not merely as a common feature, but as a pivotal, conserved signaling hub and a master regulatory switch for stress-induced lipid biosynthesis, representing a prime target for future metabolic engineering²⁴. This perspective extends recent advances in multi-omics and metabolic flux analysis, which have significantly improved our understanding of lipid accumulation in oleaginous microalgae under nitrogen stress. Under nitrogen deficiency, *Nannochloropsis oceanica* exhibits proteome-level adaptations—such as sustained photosynthesis, enhanced TCA cycle activity, and Kennedy pathway activation—that promote TAG biosynthesis²⁶. In *Nannochloropsis gaditana*, nitrogen stress leads to marked downregulation of photosynthetic and protein synthesis machinery, while upregulating key lipid-assembly proteins like DGAT²⁷. Similarly, nitrogen deprivation elevates TAG production in *Chlamydomonas reinhardtii*, with multi-omics reanalysis underscoring the central role of arginine and ornithine metabolism. Moreover, the involvement of phosphorylation, nitrosylation, and peroxidation signaling events was highlighted in the regulatory network²⁸. Thus, while prior omics studies have cataloged the metabolic components of the response, our findings position the MAPK cascade as the central signaling integrator that commands this lipid biosynthesis program under varying nitrogen stress.

Gene expression patterns underpinning growth and lipid biosynthesis under varying nitrogen deprivation

The most pronounced transcriptional response was the general downregulation of key genes involved in the Calvin cycle, including *rbcl*, *rbcs*, and *PRK*. This suppression likely reduces carbon fixation into carbohydrates and redirects the carbon flux towards the synthesis of storage lipids, a common metabolic shift under nutrient stress when growth is arrested. Concomitantly, we observed a significant upregulation of several genes in the glycolytic pathway, such as *HK*, *PFK*, and *PK*. This enhanced glycolytic activity ensures an increased supply of phosphoenolpyruvate and pyruvate, which are crucial precursors for the synthesis of acetyl-CoA, the fundamental building block for de novo fatty acid synthesis¹³.

The fate of pyruvate appears to be strategically redirected. While the gene *aceE* was upregulated, facilitating the conversion of pyruvate into acetyl-CoA, key enzymes in the TCA cycle (*CIS*, *IDH*) were repressed. This pattern suggests a bypass of the full TCA cycle, which typically supports biomass production and energy generation during active growth. Instead, the cycle may operate in a non-cyclic, “broken” mode to primarily generate citrate for export to the cytosol, where it can be cleaved to provide acetyl-CoA for lipogenesis. The upregulation of *MDH* could further support this process by generating NADH, which is essential for redox balance in lipid biosynthesis¹².

The most critical evidence for lipid hyperaccumulation comes from the dramatic upregulation of genes encoding enzymes in the Kennedy pathway and fatty acid synthesis. The key triacylglycerol (TAG) assembly enzymes—*GPAT*, *LPAAT*, *PAP*, and most notably *DGAT*—were all significantly upregulated. This concerted action channels fatty acids into TAG, the primary storage lipid. Furthermore, the rate-limiting step in fatty acid synthesis, catalyzed by *ACC*, was transcriptionally enhanced, along with other genes in the *FAS* pathway (e.g., *fabD*, *fabF*). This indicates a robust activation of the entire machinery for converting acetyl-CoA into long-chain fatty acids⁷.

In summary, our transcriptomic data delineate a coherent metabolic model (Fig. 6) for nitrogen deprivation-induced lipid accumulation: (1) carbon fixation is attenuated; (2) carbon flow is shunted through enhanced glycolysis to generate precursors; (3) The TCA cycle is remodeled to supply acetyl-CoA and reducing equivalents; and (4) The Kennedy pathway and *FAS* are transcriptionally activated to efficiently synthesize and store TAGs².

Rate-limiting steps of regulatory mechanisms at different nitrogen concentrations

Genes with similar expression patterns were classified using Short Time-series Expression Miner (STEM). The trend characteristics of gene sets in profile 9 and profile 42 were found to be related to the monotonic trend of lipid accumulation (Fig. 5). These monotonic gene sets may indicate potential rate-limiting steps in microalgal lipid accumulation under different levels of nitrogen deprivation²⁹.

The GO terms associated with tRNA processing and the COP9 signalosome showed monotonic trends in profile 9, suggesting that varying nitrogen deprivation could suppress protein biosynthesis and promote protein degradation through these processes. tRNA processing modifies the canonical L-shaped structure of tRNA through post-transcriptional modifications, which is necessary for protein synthesis¹⁵. COP9 signalosome suppresses the activity of E3 ubiquitin ligase by facilitating the cleavage of NEDD8-CUL1 conjugate (i.e. deneddylation), which prevents protein degradation³⁰. It is known that changes in the biosynthesis and degradation of proteins contribute to lipid accumulation in microalgae. In particular, when protein biosynthesis is inhibited, excess photosynthetic carbons are redirected toward triglyceride production. In addition, protein breakdown occurs in response to environmental stresses, and nitrogen salvaged is diverted to the TCA cycle for lipid biosynthesis³¹. Therefore, these protein biosynthesis and degradation processes (tRNA processing and COP9 signalosome) may serve as rate-limiting steps in lipid accumulation under varying nitrogen deprivation.

The consistent patterns of GO terms correlated with oxidized nicotinamide adenine dinucleotide (NAD⁺), thiamine pyrophosphate (TPP), succinate dehydrogenase (SDH), and pyruvate dehydrogenase (PDH) in profile 9 and profile 42 indicate that varying nitrogen deprivation may affect the TCA cycle and glycolysis through the processes associated with these crucial molecules. Oxidized nicotinamide adenine dinucleotide (NAD⁺), as a hydrogen receptor, plays important roles in the TCA cycle and glycolysis³². Thiamine pyrophosphate

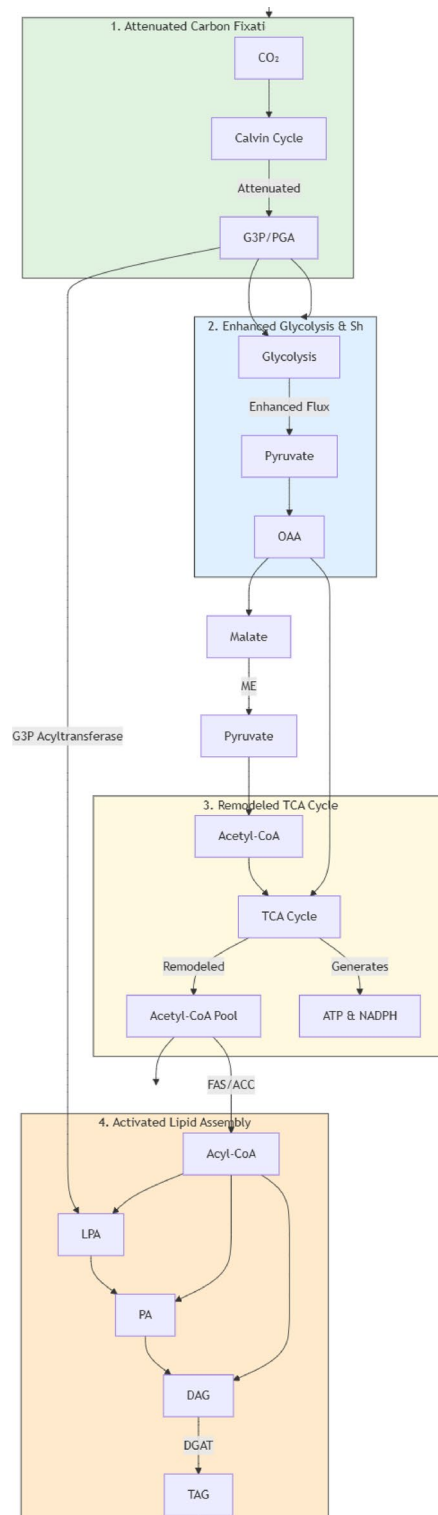


Fig. 6. The overall process of metabolic reprogramming from carbon fixation to TAG synthesis in *A. pyrenoidosa* SHOU-1002 under nitrogen deprivation.

(TPP) serves as an essential cofactor for catalytic enzymes, including α -ketose transketolase (TK, EC. 2.2.1.1) in the pentose phosphate (PPP) pathway, α -ketoglutarate dehydrogenase (KGDH, EC. 1.2.4.2) and pyruvate dehydrogenase (PDH, EC. 1.2.4.1) in TCA cycle etc³³. Succinate dehydrogenase (SDH, EC. 1.3.5.1) supplies electrons to mitochondrial electron transport chains, whose activity can generally be used as an indicator to evaluate the operational degree of the TCA cycle³⁴. Pyruvate decarboxylase (PDH, EC. 1.2.4.1) catalyzes the irreversible reaction of pyruvic acid to acetyl-CoA, which links glycolysis and TCA cycle³¹. In short, they are

crucial molecules in the TCA cycle and glycolysis. Moreover, both TCA cycle and glycolysis are associated with energy metabolism and provide carbon skeletons for lipid biosynthesis³¹. Therefore, the processes described above, which participate in the TCA cycle and glycolysis, may become rate-limiting steps of lipid accumulation in microalgae under varying nitrogen deprivation.

In this study, the response to gibberellin (GO:0009739) was the most significantly enriched GO term in profile 42. Its trend was similar to that of lipid contents. This result suggests that endogenous gibberellins may respond to varying nitrogen deprivation and affect lipid accumulation in microalgae. Gibberellins are diterpene hormones that respond to environmental stresses and affect various physiological metabolisms in plants. Upon exposure to stresses, the homeostasis of gibberellins is altered through the expression of regulatory genes³⁵. Besides, gibberellins have been reported to enhance the utilization of glucose and metabolites in the biosynthesis of fatty acids in microalgae³⁶. Therefore, it is an interesting topic to identify and explore the roles of gibberellins in the lipid accumulation of microalgae under nitrogen deprivation. However, there are few related reports available. This situation may be attributed to the immaturity of endogenous gibberellin assays in microalgae. Fortunately, Stirk et al.³⁷ first used appropriate methods to determine endogenous gibberellins in microalgae. This breakthrough may promote research on the regulation of lipid accumulation in microalgae by endogenous gibberellins.

The GO terms related to hydrolases were significantly enriched in the top 10 of profile 9 and profile 42, and their trends were monotonic. This result indicates that hydrolases in lysosomes may play a role in enhancing lipid accumulation in microalgae under varying nitrogen deprivation. Lysosomes contain hydrolases that participate in the digestion of proteins, nucleic acids and polysaccharides. This process helps achieve the turnover of substances necessary for lipid accumulation in microalgae^{38,39}. Nitrogen deprivation has been reported to induce the storage of amino acids and intermediate molecules³¹. This process may activate multiple homeostatic signaling pathways through lysosomes, leading to changes in various cellular behaviors⁴⁰. However, the roles of lysosomes and their internal hydrolases in lipid accumulation and the underlying mechanisms seem to be overlooked. Additional research is needed.

Conclusions

The distinct characteristics of lipid accumulation in *A. pyrenoidosa* under varying nitrogen deprivation were changes in nitrogen assimilation, chloroplast metabolism and nucleolar stress. In addition, the common characteristics were the variations in the TCA cycle, MAPK cascade and transporter. Moreover, the processes related to tRNA processing, COP9 signalosome, TCA cycle, glycolysis, gibberellins and lysosomes were possible rate-limiting steps. Notably, the pivotal role of the consistently activated MAPK cascade makes its exploration a priority for future metabolic engineering.

Data availability

The raw data of transcriptome in this study has been submitted to the National Center for Biotechnology Information (Accession number: GSE233967). Other data is available from the corresponding author on request.

Received: 9 June 2025; Accepted: 13 November 2025

Published online: 21 November 2025

References

- Greene, J. M., Quiroz, D., Limb, B. J. & Quinn, J. C. Geographically-Resolved Techno-Economic and life cycle assessment comparing Microalgae-Based renewable diesel and sustainable aviation fuel in the united States. *Environ. Sci. Technol.* **59**, 3472–3483 (2025).
- Singh, R. P. et al. Unlocking the adaptation mechanisms of the oleaginous microalga *Scenedesmus* sp. BHU1 under elevated salt stress: a physiochemical, lipidomics and transcriptomics approach. *Front. Microbiol.* **15**, 1475410 (2024).
- Usman, H. M. et al. Comparative analysis assessing growth dynamics of locally isolated *Chlorella Sorokiniana* and *Chlorella vulgaris* for biomass and lipid production with biodiesel potential. *Bioresour Technol.* **403**, 130868 (2024).
- Pandey, S., Narayanan, I., Selvaraj, R., Varadavenkatesan, T. & Vinayagam, R. Biodiesel production from microalgae: a comprehensive review on influential factors, transesterification processes, and challenges. *Fuel* **367**, 131547 (2024).
- Kossalbayev, B. D. et al. Strategies for genetic modification of microalgae to improve the production efficiency of liquid biofuel. *Int. J. Hydrogen Energ.* **100**, 1301–1314 (2025).
- Yan, C. X. et al. Advances in multi-omics technologies for identifying metabolic engineering targets and improving lipid production in microalgae. *Bioresour Technol.* **429**, 132501 (2025).
- de Jesús-Campos, D. et al. Chemical composition, fatty acid profile and molecular changes derived from nitrogen stress in the diatom *Chaetoceros muelleri*. *Aquac Rep.* **16**, 100281 (2020).
- Kiran, B., Pathak, K., Kumar, R., Deshmukh, D. & Rani, N. Influence of varying nitrogen levels on lipid accumulation in *Chlorella* Sp. *Int. J. Environ. Sci. Te.* **13**, 1823–1832 (2016).
- Huang, X. X., Huang, Z. Z., Wen, W. & Yan, J. Q. Effects of nitrogen supplementation of the culture medium on the growth, total lipid content and fatty acid profiles of three microalgae (*Tetraselmis subcordiformis*, *Nannochloropsis oculata* and *Pavlova viridis*). *J. Appl. Phycol.* **25**, 129–137 (2013).
- Sibi, G., Shetty, V. & Mokashi, K. Enhanced lipid productivity approaches in microalgae as an alternate for fossil fuels—a review. *J. Energy Inst.* **89**, 330–334 (2016).
- Wang, X. X., Fosse, H. K., Li, K., Chauton, M. S. & Reitan, K. I. Influence of nitrogen limitation on lipid accumulation and EPA and DHA content in four marine microalgae for possible use in Aquafeed. *Front. Mar. Sci.* **6**, 95 (2019).
- Jaeger, D. et al. Time-resolved transcriptome analysis and lipid pathway reconstruction of the oleaginous green microalga *Monoraphidium neglectum* reveal a model for triacylglycerol and lipid hyperaccumulation. *Biotechnol. Biofuels.* **10**, 197 (2017).
- Bonnefond, H. et al. Coupling and uncoupling of triglyceride and beta-carotene production by *Dunaliella Salina* under nitrogen limitation and starvation. *Biotechnol. Biofuels.* **10**, 25 (2017).
- Liu, J. Y., Qiu, W. & Song, Y. M. Stimulatory effect of auxins on the growth and lipid productivity of *Chlorella pyrenoidosa* and *Scenedesmus quadricauda*. *Algal Res.* **18**, 273–280 (2016).

15. Wei, W., Zhuang, H., Zhang, Y. & Wang, L. Crustacean zooplankton community in relation to physicochemical factors and phytoplankton of 13 waterbodies located in the Yangtze river delta. *Ann. Limnol-Int J. Lim.* **55**, 16 (2019).
16. Zhang, Y. et al. Dose-dependent effects of polystyrene nanoplastics on growth, photosynthesis, and Astaxanthin synthesis in *Haematococcus pluvialis*. *Environ. Pollut.* **359**, 124574 (2024).
17. Kanehisa, M., Sato, Y., Kawashima, M., Furumichi, M. & Tanabe, M. KEGG as a reference resource for gene and protein annotation. *Nucleic Acids Res.* **44**, D457–D462 (2016).
18. Kanehisa, M. & Goto, S. KEGG: Kyoto encyclopedia of genes and genomes. *Nucleic Acids Res.* **28**, 27–30 (2000).
19. Gupta, N., Khare, P. & Singh, D. P. Nitrogen-dependent metabolic regulation of lipid production in microalga *Scenedesmus vacuolatus*. *Ecotoxicol. Environ. Saf.* **174**, 706–713 (2019).
20. Stephenson, P. G., Moore, C. M., Terry, M. J., Zubkov, M. V. & Bibby, T. S. Improving photosynthesis for algal biofuels: toward a green revolution. *Trends Biotechnol.* **29**, 615–623 (2011).
21. Wu, J. Y. et al. PHA-4/FoxA senses nucleolar stress to regulate lipid accumulation in *Caenorhabditis elegans*. *Nat. Commun.* **9**, 1195 (2018).
22. Woodson, J. D. & Chory, J. Coordination of gene expression between organellar and nuclear genomes. *Nat. Rev. Genet.* **9**, 383–395 (2008).
23. Yang, Z. K., Niu, Y. F., Ma, Y. H. & Jiao, X. Molecular and cellular mechanisms of neutral lipid accumulation in diatom following nitrogen deprivation. *Biotechnol. Biofuels.* **6**, 67–67 (2013).
24. Wang, L. F., Ming, D., Pan, Y. Y., Shi, L. Q. & Wei, W. Z. Nitrogen limitation and hydrogen peroxide act synergistically to enhance lipids accumulation via ROS/Ca²⁺ dependent mechanism in *Chlorella Sorokiniana*. *Algal Res.* **70**, 102974 (2023).
25. Zhang, S., He, Y., Sen, B. & Wang, G. Reactive oxygen species and their applications toward enhanced lipid accumulation in oleaginous microorganisms. *Bioreour Technol.* **307**, 123234 (2020).
26. You, W. et al. Integration of proteome and transcriptome refines key molecular processes underlying oil production in *Nannochloropsis oceanica*. *Biotechnol. Biofuels.* **13**, 109 (2020).
27. Hulatt, C. J. et al. Proteomic and transcriptomic patterns during lipid remodeling in *Nannochloropsis Gaditana*. *Int. J. Mol. Sci.* **21**, 6946 (2020).
28. Monteiro, L. F. R., Giraldi, L. A. & Winck, F. V. From feasting to fasting: the arginine pathway as a metabolic switch in nitrogen-deprived *Chlamydomonas reinhardtii*. *Cells* **12**, 1379 (2023).
29. Ernst, J. & Bar-Joseph, Z. Stem: a tool for the analysis of short time series gene expression data. *BMC Bioinform.* **7**, 191 (2006).
30. Qin, N. X., Xu, D. Q., Li, J. G. & Deng, X. W. COP9 signalosome: Discovery, conservation, activity, and function. *J. Integr. Plant. Biol.* **62**, 90–103 (2020).
31. Chen, H., Zheng, Y. L., Zhan, J., He, C. & Wang, Q. Comparative metabolic profiling of the lipid-producing green microalga *Chlorella* reveals that nitrogen and carbon metabolic pathways contribute to lipid metabolism. *Biotechnol. Biofuels.* **10**, 153 (2017).
32. Noctor, G., Hager, J. & Li, S. Biosynthesis of NAD and its manipulation in plants. *Adv. Bot. Res.* **58**, 153–201 (2011).
33. Rosado-Souza, L. et al. Appropriate Thiamin pyrophosphate levels are required for acclimation to changes in photoperiod. *Plant. Physiol.* **180**, 185–197 (2019).
34. Affourtit, C., Krab, K., Leach, G. R., Whitehouse, D. G. & Moore, A. L. New insights into the regulation of plant succinate dehydrogenase. On the role of the protonmotive force. *J. Biol. Chem.* **31**, 276, 32567–32574 (2001).
35. Yamaguchi, S. Gibberellin metabolism and its regulation. *Annu. Rev. Plant. Biol.* **59**, 225–251 (2008).
36. Yu, X. J., Sun, J., Sun, Y. Q., Zheng, J. Y. & Wang, Z. Metabolomics analysis of phytohormone Gibberellin improving lipid and DHA accumulation in *Aurantiochytrium* Sp. *Biochem. Eng. J.* **112**, 258–268 (2016).
37. Stirk, W. A. et al. Hormone profiles in microalgae: gibberellins and brassinosteroids. *Plant. Physiol. Bioch.* **70**, 348–353 (2013).
38. De Duve, C. & Wattiaux, R. Functions of lysosomes. *Annu. Rev. Physiol.* **28**, 435–492 (1966).
39. Nagappan, S. et al. Metabolomics integrated with transcriptomics and proteomics: evaluation of systems reaction to nitrogen deficiency stress in microalgae. *Process. Biochem.* **91**, 1–14 (2020).
40. Zhang, Z. Q. et al. Role of lysosomes in physiological activities, diseases, and therapy. *J. Hemato Oncol.* **14**, 79 (2021).

Acknowledgements

We thank Jingyuan Ge and Lihui Gao in OEbiotech.co.ltd for technical support in the transcriptome analysis of this study.

Author contributions

Writing-original draft preparation, W.L.F. Conceptualization, W.L.F. Methodology, M.X.Y. Investigation, H.X.X. Validation, W.H.B. Formal analysis, J.W. Resources, C.W.W. Data Curation, W.Y.F. Writing-review and editing, X.P. Visualization, W.L.F. Supervision, W.H.B. and H.X.X. Project administration, W.H.B. and H.X.X. Funding acquisition, W.L.F. All authors reviewed the manuscript.

Funding

This research was primarily supported by grants from the Central Public-interest Scientific Institution Basal Research Fund, Freshwater Fisheries Research Center, CAFS (NO. 2025JBFR06). Additional support was provided by the Natural Science Foundation of China (31800435).

Declarations

Competing interests

The authors declare no competing interests.

Additional information

Supplementary Information The online version contains supplementary material available at <https://doi.org/10.1038/s41598-025-28963-x>.

Correspondence and requests for materials should be addressed to H.X. or W.H.

Reprints and permissions information is available at www.nature.com/reprints.

Publisher's note Springer Nature remains neutral with regard to jurisdictional claims in published maps and institutional affiliations.

Open Access This article is licensed under a Creative Commons Attribution-NonCommercial-NoDerivatives 4.0 International License, which permits any non-commercial use, sharing, distribution and reproduction in any medium or format, as long as you give appropriate credit to the original author(s) and the source, provide a link to the Creative Commons licence, and indicate if you modified the licensed material. You do not have permission under this licence to share adapted material derived from this article or parts of it. The images or other third party material in this article are included in the article's Creative Commons licence, unless indicated otherwise in a credit line to the material. If material is not included in the article's Creative Commons licence and your intended use is not permitted by statutory regulation or exceeds the permitted use, you will need to obtain permission directly from the copyright holder. To view a copy of this licence, visit <http://creativecommons.org/licenses/by-nc-nd/4.0/>.

© The Author(s) 2025